GIS-BASED SPATIAL BIAS ADJUSTMENT OF RADAR-DERIVED RAINFALL ESTIMATES DURING STORM DISSIPATION IN CENTRAL THAILAND

Apichaya KANGERD [1] ***& Nattapon MAHAVIK*** [1,2*]

DOI: 10.21163/GT_2026.211.13

ABSTRACT

Thailand lies in a tropical monsoon region and is frequently affected by the decay of tropical storms during the rainy season, with 2–5 storms typically occurring each year. Accurate quantitative precipitation estimates (QPE) are therefore essential for assessing storm-related rainfall and associated flood risks. Radar-based rainfall estimation is particularly suitable but is prone to systematic bias arising from the radar reflectivity–rainfall (Z–R) relationship. This study develops a Geographic Information System (GIS)-based analytical approach to evaluate and compare Z–R relationships and to reduce bias between radar-estimated and gauge-observed rainfall. The analysis was conducted across lowland and mountainous areas in northern and central Thailand using data from the Phitsanulok C-band weather radar and 89 rain gauge stations during Tropical Storm Son-Tinh (2018). This study integrates radar data with Geographic Information Systems (GIS) to systematically compare multiple Z–R relationships alongside spatial bias correction, and to evaluate differences in rainfall estimation accuracy between lowland and mountainous areas. Three Z–R relationships Marshall–Palmer (MP), Rosenfeld Tropical (RF), and Summer Deep Convection (SD) were employed to generate event-based radar rainfall estimates. Spatial bias correction was conducted using the Inverse Distance Weighting (IDW) method, and accuracy was assessed through five-fold cross-validation. The results indicate that uncorrected radar rainfall estimates generally underestimate actual precipitation, whereas the IDW-based correction significantly reduces the Mean Field Bias (MFB) and improves estimation accuracy across diverse terrains. Among the three Z–R relationships, the Marshall–Palmer equation yielded the lowest errors, with a root mean square error (RMSE) of 17.517 mm and a mean absolute error (MAE) of 13.405 mm. The event-based spatial adjustment demonstrates that integrating an appropriate Z–R relationship with GIS-based bias correction substantially enhances radar QPE reliability, particularly in regions with complex topography. This framework offers practical value for hydrological applications and flood risk management in tropical monsoon regions.

Keywords: *Quantitative Precipitation Estimation (QPE); Bias correction; GIS-based analysis; Tropical Storm Son-Tinh.*

1. INTRODUCTION

Thailand was among the countries in Southeast Asia that were impacted by Tropical Storm Son-Tinh in July 2018. The storm resulted in substantial damage to infrastructure and agriculture, notably in the northeastern and northern regions of Thailand, as well as flash floods, widespread inundation, and heavy rainfall (Thai Meteorological Department, 2018; National Water Resources Agency, 2018). The predominance of convective clouds over stratiform clouds was observed in radar-based analyses of storm decomposition in central Thailand, as evidenced by multi-station radar mosaics (Mahavik & Tantanee, 2020a). This incident underscores the significance of accurate rainfall estimation in the context of disaster management and early warning systems. However, because spatial bias varies across different radar rainfall relationships, applying spatial bias correction may improve radar rainfall estimates within the water basin. Accordingly, this study investigates whether such correction can enhance the accuracy of radar-derived rainfall.

[1]*Department of Natural Resources and Environment, Faculty of Agriculture Natural Resources and Environment, Naresuan University, Phitsanulok 65000, Thailand, apichayakan66@nu.ac.th*
[2]*Water Resources Research Center, Faculty of Engineering, Naresuan University, Phitsanulok 65000, Thailand,*
**Corresponding author: nattaponm@nu.ac.th*

The spatial resolution and reliability of precipitation data are critical factors in the study of floods and rainfall. The upper Chao Phraya basin and its tributaries Ping, Wang, Yom, and Nan are distinguished by their complex topography, which encompasses narrow valleys, foothills, and ridges. Abro et al. (2019) have demonstrated that highland regions typically receive a greater amount of annual rainfall than lowlands. However, satellite-based precipitation products frequently underestimate rainfall in these regions, particularly during severe storms with highly heterogeneous precipitation rates. The sparse and uneven distribution of ground-based rain gauges results in high uncertainty in rainfall datasets, despite the fact that they provide precise point-scale measurements (Brauer et al., 2016). This is due to the fact that mountainous and remote areas are underrepresented.

Weather radar provides spatially and temporally detailed rainfall observations that are appropriate for medium to small basins (Harrison et al., 2009). Nevertheless, radar measurements are susceptible to a variety of sources of uncertainty, such as attenuation, anomalous propagation, ground clutter, calibration errors, partial beam blockage, and bright band contamination (Gourley & Calvert, 2003; Krajewski et al., 2010; Krajewski et al.,2011; Sharif et al., 2020; Mahavik et al., 2025). The quality of radar echoes is further compromised by clutter from communication towers, towering buildings, or mountains, resulting in the misclassification of non-precipitation signals as rainfall (Mahavik et al., 2025). Nevertheless, the integration and processing of multi-station radar data have been demonstrated to improve rainfall monitoring in storm decay events across vast basins, despite these challenges (Mahavik & Tantanee, 2020; Mahavik et al., 2025).

The relationship between radar reflectivity and rainfall rate (Z–R relationship) is a fundamental component of radar-based quantitative precipitation estimation (QPE), as it provides the empirical link between radar reflectivity (Z) and the surface rainfall rate (R). The Z–R relationship is not universal; rather, it varies depending on factors such as drop size distribution (DSD), storm type, and topographic conditions (Morin et al., 2003; Wu et al., 2018). Accurate QPE therefore requires selecting an appropriate Z–R relationship that best represents the rainfall characteristics of each region. The Marshall–Palmer (MP) (Marshall & Palmer, 1948), Rosenfeld Tropical (RF) (Rosenfeld et al., 1993), and Summer Deep Convection (SD) (Battan, 1973) equations are widely used examples that represent distinct environmental and microphysical rainfall characteristics. Specifically, the MP relationship is most suitable for stratiform rainfall characterized by small raindrop sizes, the RF for tropical convective rainfall typical of humid climates, and the SD for deep convective rainfall associated with intense summer thunderstorms.

Radar-based rainfall estimates are frequently combined with rain gauge data to rectify systematic biases, thereby further reducing uncertainties. Spatial interpolation and other bias correction techniques are employed to mitigate the discrepancy between radar areal estimates and point-scale gauge observations (Ahrens, 2006; Mahavik, 2017; Mapium et al., 2022). Geographic Information Systems (GIS) offer robust instruments for the integration of spatial data, the management of rainfall fields, and the application of bias correction techniques, thereby increasing the value of radar datasets for hydrological and meteorological applications (Xie et al., 2005; Cho, 2020; Mahavik et al., 2021).

Therefore, the integration of radar-based rainfall estimates with ground-based rain gauge measurements, which can be effectively implemented through Geographic Information Systems (GIS), is crucial for enhancing rainfall estimation accuracy, particularly in regions with complex terrain. This study systematically applies atmospheric radar data in conjunction with GIS in the central region of Thailand to analyze rainfall associated with Tropical Storm Son-Tinh (2018). Radar data were obtained from the Phitsanulok C-band radar station, while rainfall measurements were collected from 89 ground-based rain gauge stations. The primary objective was to evaluate the suitability of three Z–R relationships: Summer Deep Convection (SD), Rosenfeld Tropical (RF), and Marshall–Palmer (MP). To address spatial bias, the Inverse Distance Weighting (IDW) method was applied, and the estimation accuracy was assessed using five-fold cross-validation to examine the consistency between radar-derived rainfall and gauge observations. Accuracy was further evaluated using two categories of statistical metrics: (1) error-based measures, including Root Mean Square Error (RMSE) and Mean Absolute Error (MAE), and (2) bias-based measures, such as Mean Field Bias (MFB).

2. STUDY AREA

The ground-based weather radar at the Phitsanulok Weather Radar Station, operated by the Thai Meteorological Department, is located at an elevation of 47 meters above mean sea level (MSL) at geographic coordinates 16.775531°N, 100.217901°E, as shown in **Fig. 1** The radar operates in the C-band frequency with an observation radius of 240 km and performs four scans per hour at elevation angles of 0.5°, 1.5°, 2.4°, and 3.4° (Kangerd et al., 2024; Mahavik et al., 2025). The area covered by the weather radar encompasses diverse topography, ranging from flood-prone lowland plains in the central and southern regions to mountainous terrain distributed along the western, northern, and eastern edges of the radar detection range. This region also includes key river basins within the Chao Phraya watershed, such as the Ping, Wang, Yom, and Nan rivers. In mid-July, the study area experienced intense rainfall and flooding associated with Tropical Storm Son-Tinh, which moved from Vietnam into the upper northeastern region of Thailand, coinciding with a strong southwest monsoon. The combination of the storm and monsoon resulted in prolonged heavy rainfall, particularly over the upper northern and northeastern regions. Consequently, this event was selected as a case study within a 120-kilometer radar observation radius.

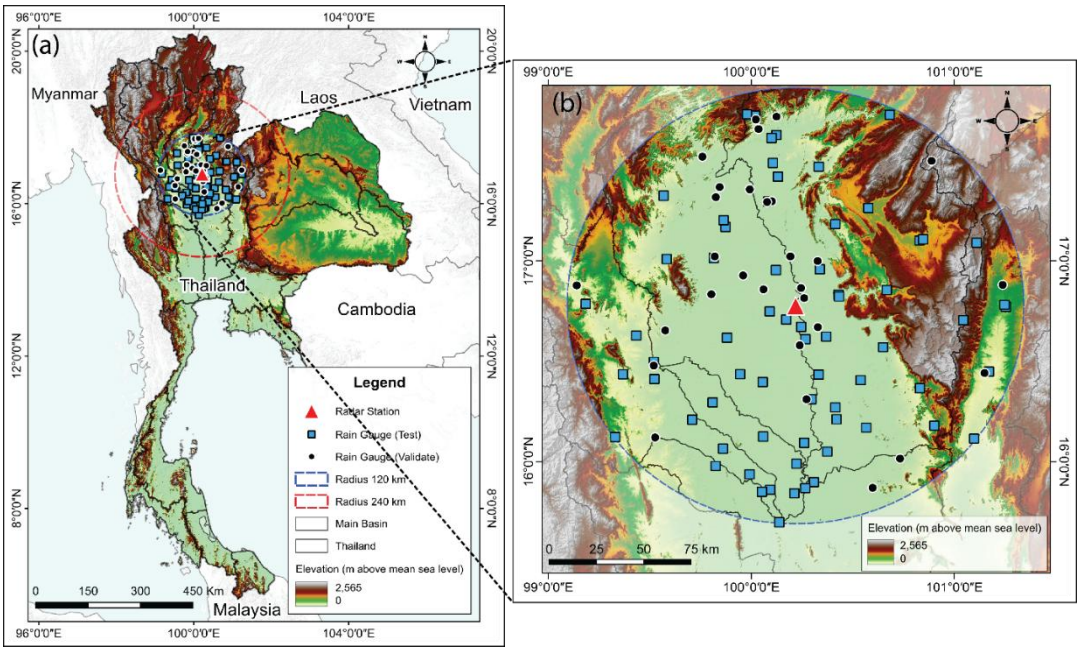

Fig. 1. Study area: (a) the national boundary of Thailand; (b) the observational domain of the Phitsanulok weather radar within the Chao Phraya Basin. The red triangle denotes the location of the radar station. The blue dashed circle represents the radar's observation coverage with a radius of 120 kilometers. Blue squares with black outlines indicate the locations of ground-based rain gauge stations used as the testing dataset, while black circles with white outlines represent the validation dataset. In total, 89 rain gauge stations were employed in this study.

3. DATA AND METHODS

3.1. Radar Data Observed by Ground-Based Radar Station

In order to minimize uncertainty and more accurately represent near-surface rainfall, radar data at the lowest available elevation angles were chosen for this investigation, as per the methodology of Kangerd et al. (2024). To analyze the rainfall associated with Tropical Storm Son-Tinh over a nine-day period (15–23 July 2018), a Constant Altitude Plan Position Indicator (CAPPI) was generated at 2 km above mean sea level. The Thai Meteorological Department (TMD) operates the Phitsanulok Weather Radar Station in Thailand (16.775531°N, 100.217901°E; 47 m a.s.l.), from which the data

were obtained. This C-band dual-polarization radar has a 240 km observation radius, which allows it to cover lower northern and central Thailand. It conducts scans every 15 minutes (four times per hour) at elevation angles of 0.5°, 1.5°, 2.4°, and 3.4° (Mahavik et al., 2025). Only daily accumulated rainfall files with a scan availability of at least 80% (≥19 hours of data per day) were retained for quality control. All 825 radar files that met these criteria have been used in the analysis.

3.2. Rain gauge rainfall data

Within a 120 km radar observation radius, rainfall data and station locations were obtained from the Automatic Telemetry Stations of the Water Resources Information Institute (Public Organization; WRI). It is imperative to resolve radar limitations, including signal attenuation with distance and beam broadening, which can result in a discrepancy between radar reflectivity and actual ground rainfall (Mahavik et al., 2024). These stations are thus crucial. The WRI API was used to access the data in CSV format (https://tiservice.hii.or.th/opendata/data_catalog/hourly_rain/0all_stn_meta data. csv) for the duration of Tropical Storm Son-Tinh, local Thailand time. After quality control and the removal of anomalous or lacking data, 89 stations were chosen for the study in accordance with the gauge-density standards of the World Meteorological Organization (2008), as shown in **Fig. 1b** Initially, 96 stations were considered. We employed these hourly rainfall data as ground truth for the bias correction procedure, comparing them to radar-derived rainfall.

3.3. Digital elevation model (DEM)

A 30-meter spatial resolution Digital Elevation Model (DEM) from the United States Geological Survey (USGS) was used. The researchers developed code to classify areas based on slope values derived from the DEM. The slope classification was adapted from Mokarram & Hojati (2016), where areas with slopes $\leq 5^{\circ}$ were defined as flat or lowland (Class 1), and those $>5^{\circ}$ as hilly or mountainous (Class 2), with no-data areas assigned as Class 0. The resulting raster-based classification (lowland vs. mountainous) was then converted into vector format for GIS-based spatial analysis.

3.4. Software and Libraries

Data analysis was conducted using Python. The open-source Py-ART library (Helmus & Collis, 2016) was employed for processing and analyzing ground-based radar data and is fully compatible with other Python libraries, including NumPy, Scikit-learn, Matplotlib, CartoPy, and Xarray (Bowden et al., 2025; Mahavik et al., 2024, 2025). Py-ART was specifically used for filtering and removing signal noise (Signal-to-Noise Ratio: SNR) and for attenuation correction using dual-polarimetric variables, which compensates for signal weakening with distance and improves radar observations of convective cloud systems in the C-band radar (Gu et al., 2011), providing accurate input for rainfall estimation. Open-source GIS software QGIS (QGIS Development Team, 2024) was used for geospatial visualization of radar data, both in preliminary data preparation and spatial analysis. In this study, a workflow was developed in QGIS to process accumulated rainfall, facilitating efficient handling of both spatial and temporal data for subsequent analyses.

3.5. Z-R relationships

The Z–R relationship, which describes the correlation between radar reflectivity and rainfall rate, is used to estimate rainfall from radar reflectivity measurements. Radar reflectivity, representing the scattering of radar waves by raindrops in the atmosphere, cannot directly indicate the amount of rainfall reaching the ground, unlike ground-based rain gauge measurements. Therefore, radar reflectivity (Z), measured in dBZ, must be converted into rainfall rate (R) (Mahavik et al., 2021; Mapiam & Sriwongsitanon, 2008) using a power-law relationship, as expressed in Eq. (1)

$$Z = aR^b \tag{1}$$

where, Z denotes the radar reflectivity factor, expressed in units of (mm6 /m^{-3}) while R represents the rainfall rate, expressed in (mm/h). Constants a and b (**Table 1**.) are empirical coefficients that depend on the raindrop size distribution and may vary according to rainfall characteristics, precipitation type, and seasonal conditions. In Thailand, commonly adopted coefficient values have been defined for operational use.

Table 1.

Z–R relationships used for converting radar reflectivity to rainfall rate.

Z-R relationship	Equation	Description
Marshall/Palmer (MP)	$Z = 200R^{1.6}$	Represents stratiform rainfall events or small raindrop sizes in mid-latitudes (Marshall & Palmer, 1948).
Rosenfeld Tropical (RF)	$Z = 250R^{1.2}$	Represents rainfall events in tropical regions (Rosenfeld et al., 1993).
Summer Deep Convection (SD)	$Z = 300R^{1.4}$	Represents convective rainfall events associated with vertically developed clouds or intense convective storms during summer (Battan, 1973).

3.6. Evaluation metrics

In order to assess the performance of radar-estimated rainfall in comparison to ground-based measurements, three statistical metrics were used: Root Mean Square Error (RMSE) and Mean Absolute Error (MAE), which quantify the magnitude of differences between radar and observed rainfall, and Mean Field Bias (MFB), which evaluates whether radar rainfall tends to systematically overestimate or underestimate rainfall relative to gauge observations. Based on Mahavik et al. (2024), these statistics are frequently employed to assess the discrepancies between observed and model-derived data. MFB is a method that is frequently employed in meteorological research to evaluate the accuracy and bias of radar precipitation estimates. It is specifically used to evaluate the difference between radar-estimated rainfall (RR) and gauged rainfall (GR).

3.6.1. Root mean squared error: RMSE

RMSE is a statistical measure used to quantify the magnitude of errors in estimated rainfall compared with ground observations. It is computed by squaring the differences between radar and gauge rainfall, averaging these squared differences, and then taking the square root of the mean. RMSE therefore reflects the average magnitude of error in quantitative terms. Because squaring emphasizes larger deviations, substantial errors exert greater influence on the RMSE than smaller ones. The RMSE is expressed as Eq. (2)

$$\mathrm{RMSE} = \sqrt{\frac{1}{n}\sum_{i=1}^{n}(\mathrm{GR_i} - \mathrm{RR_i})^2} \tag{2}$$

3.6.2. Mean absolute error: MAE

MAE is a statistical index used to assess the accuracy of radar-estimated rainfall by comparing it against ground-based observations. It is calculated as the mean of the absolute differences between radar estimates and gauge measurements. Unlike RMSE, MAE does not disproportionately weight larger errors, thereby providing a balanced representation of the average magnitude of discrepancies, regardless of whether they result from overestimation or underestimation. This property makes MAE a neutral and intuitive measure of the average difference between radar and ground rainfall. The MAE is expressed as Eq. (3)

$$\mathrm{MAE} = \frac{1}{n}\sum_{i=1}^{n}|\mathrm{GR_i} - \mathrm{RR_i}| \tag{3}$$

3.6.3. Mean field bias: MFB

MFB is a fundamental technique used to adjust systematic multiplicative biases in radar-derived rainfall estimates. This metric is critical for improving the accuracy of rainfall estimation derived from radar reflectivity (Hanchoowong et al., 2012). Following Krajewski & Smith (2002), MFB is calculated by dividing the accumulated radar-estimated rainfall over a given period by the accumulated gauge-measured rainfall for the same period. An MFB value greater than 1 indicates that radar estimates tend to underestimate actual rainfall, while an MFB value less than 1 indicates that radar estimates tend to overestimate rainfall relative to ground observations. The formulation is given in Eq. (4)

$$\mathrm{MFB} = \frac{\sum_{i=1}^{n} \mathrm{GR_i}}{\sum_{i=1}^{n} \mathrm{RR_i}} \tag{4}$$

where GR_i represents the accumulated rainfall from a ground-based gauge at observation point i, and RR_i denotes the corresponding radar-estimated rainfall covering that point.

3.7. Spatial Interpolation

Spatial interpolation is commonly applied in meteorology to reduce biases in radar-estimated rainfall by integrating point-scale gauge measurements with spatially continuous radar data. In general, interpolation estimates rainfall values at unsampled locations using information from surrounding stations, thereby addressing the sparse or uneven distribution of rain gauges. Among deterministic approaches, which are widely used for bias correction, Inverse Distance Weighting (IDW) is particularly well established. IDW assumes that observations closer to the target location exert greater influence than those farther away, making it suitable for local rainfall adjustment (Chang & Kang-tsung, 2002). Previous studies have demonstrated its effectiveness: Ahrens (2006) highlighted its utility in producing daily rainfall maps and filling missing values in time series, while Chen & Liu (2012) successfully applied IDW for spatial rainfall interpolation in complex environments. More recently, Sokol et al. (2021) emphasized the relevance of deterministic methods such as IDW for radar–gauge integration. In this study, IDW was employed as a deterministic bias-correction technique to adjust radar-estimated rainfall against gauge observations. The formulation used is presented in Eq. (5) and Eq. (6)

$$\hat{R}_p = \sum_{i=1}^{N} w_i R_i \tag{5}$$

$$w_i = \frac{d_i^{-\alpha}}{\sum_{i=1}^{N} d_i^{-\alpha}} \tag{6}$$

where $\hat{R}_p$ is the unknown rainfall at location p (mm), R_i is the observed rainfall at the i ground station (mm), N is the number of stations used for interpolation, w_i is the weight assigned to station i, d_i is the distance from station i to the radar pixel, and α is the power parameter controlling the influence of distance, typically set to 2 (Kangerd et al., 2024; Lin & Yu, 2008).

3.8. K-Fold Cross-Validation

To assess the robustness of radar rainfall adjustment against ground-based observations, a K-fold cross-validation framework was implemented. Cross-validation is widely used to evaluate model performance by partitioning the dataset into multiple folds, thereby reducing dependence on a single train–test split and minimizing bias. In this study, the rain gauge dataset comprising 89 stations was randomly divided into five folds (K = 5) using QGIS tools. For each iteration, approximately 70% of the stations were assigned to the calibration subset and 30% to the validation subset. This procedure ensured that all stations were used for both calibration and validation across different folds, providing a reliable measure of model stability and accuracy.

3.9. Radar data correction

Removal of Clutter and Noise (Signal-to-Noise Ratio: SNR). Raw radar reflectivity data were preprocessed to remove contamination from non-meteorological sources, such as ground clutter, using the open-source Py-ART library (Helmus & Collis, 2016). SNR was calculated for each radar gate, and a gate filter was applied to exclude values below 1 dBZ or above 70 dBZ. These thresholds were selected to eliminate anomalous signals typically associated with clutter or spurious atmospheric variability. The Top of Atmosphere (TOA) parameter was set to 15,000 m to further suppress non-meteorological echoes.

Because C-band radar is highly sensitive to signal attenuation, which increases with both propagation distance and rainfall intensity, and because the study area contains mountain ranges that cause partial and complete beam blockage, resulting in reduced returned reflectivity (Mahavik & Tantanee, 2020b), an attenuation correction was also applied to the reflectivity field (Gu et al., 2011). After correction, the data were considered most reliable within a 120 km range, where radar estimates exhibited the highest consistency with ground-based rainfall observations (Mahavik et al., 2025). The establishment of the 120 km radar coverage boundary is based on the technical limitations of the C-band radar system and the degradation of reflectivity signal quality with increasing distance, primarily due to noise contamination and attenuation effects. As the radar beam propagates farther from the radar site, beam broadening and loss of spatial resolution become significant, leading to reduced radar performance and decreased accuracy in quantitative precipitation estimation (QPE), consistent with the findings of Mahavik et al. (2025). together, these preprocessing steps clutter, and noise filtering, TOA adjustment, and attenuation correction were essential to ensure that the reflectivity inputs used in Z–R rainfall estimation were physically consistent and of high quality.

3.10. Workflow of data analysis

The data analysis framework of this study comprised four main steps: (1) data collection, (2) data processing, (3) development of analytical methods in GIS, and (4) data analysis (**Fig. 2**).

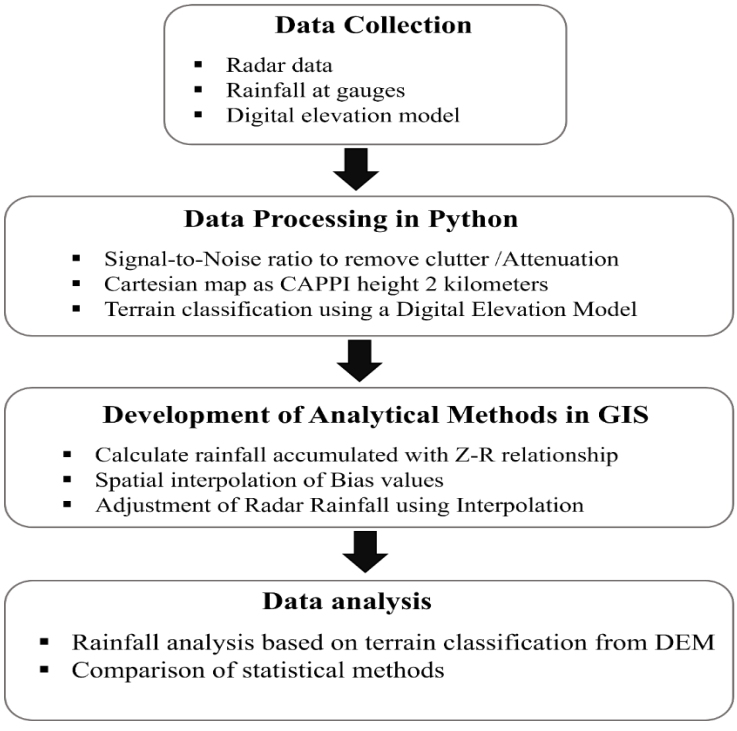

Fig. 2. Conceptual framework of the research workflow.

Data Collection. Three types of data were used: radar observations, ground-based rainfall measurements, and topographic information. Radar data were obtained from the Phitsanulok C-band ground-based weather radar operated by the Thai Meteorological Department. Four elevation angles (0.5°, 1.5°, 2.3°, and 3.4°) were selected for the period 15–23 July 2018, covering the passage of Tropical Storm Son-Tinh. To ensure temporal completeness, only days with at least 80% scan availability (≥19 hours) (Mahavik et al., 2025) were retained, resulting in 825 UF-format files recorded in UTC. Rainfall data were collected from 96 automatic telemetry stations within a 120 km radius of the radar. After quality control and removal of abnormal stations, 89 stations were retained. Data were retrieved via a Python API and synchronized to local Thai time, following the approach of Kangerd et al. (2024) to ensure temporal consistency with radar scans. Topographic information was derived from a USGS Digital Elevation Model (DEM) with 30 m resolution. The DEM was used to classify terrain into three categories: flat (slope ≤ 5°), mountainous (slope > 5°), and no-data areas.

Data Processing. Radar data were preprocessed using Python and the open-source Py-ART library (Helmus & Collis, 2016). The procedure included ground clutter filtering, attenuation correction, and transformation from polar to Cartesian coordinates. Reflectivity fields were converted into rainfall products in Constant Altitude Plan Position Indicator (CAPPI) format at 2 km altitude, generated for four scans per hour (00, 15, 30, and 45 minutes). The outputs were exported as GeoTIFF files for further spatial analysis in QGIS.

Development of Analytical Methods in GIS. A rainfall estimation and bias-correction model was implemented in GIS using the Processing Modeler. This design improved efficiency and minimized redundancy in data handling. Radar reflectivity (Z) was converted into rainfall rate (R) using three Z–R relationships: Marshall–Palmer (Marshall & Palmer, 1955), Rosenfeld Tropical (Rosenfeld et al., 1993), and Summer Deep Convection (Battan, 1973). Radar rainfall was aggregated into hourly, daily, and event-based totals, with values extracted at gauge locations (30% validation stations) for evaluation prior to bias correction. Model performance was assessed using five-fold cross-validation (K = 5), implemented in QGIS with a 70:30 calibration–validation split. Spatial bias correction was conducted by interpolating gauge‑radar differences using Inverse Distance Weighting (IDW) with the search radius and the number of interpolation points set according to the software defaults. The Distance coefficient (P) was tested from 1 to 6 using K-fold cross-validation, and model accuracy was evaluated based on RMSE, MAE, and correlation. It was found that P = 2 produced the optimal results after bias correction. (Kangerd et al., 2024) Corrected rainfall fields were subsequently re-extracted at validation stations for post-correction analysis.

Data Analysis. Spatial error patterns were analyzed in QGIS by comparing radar–gauge discrepancies across DEM-derived terrain classes. Accuracy was assessed using error metrics RMSE and MAE as well as bias metrics including MFB. These analyses provided a systematic evaluation of radar rainfall estimates before and after bias correction. Kangerd et al. (2024).

4. RESULTS AND DISCUSSIONS

4.1. Radar data correction process

The preprocessing workflow that was performed to the radar reflectivity data is shown in **Fig. 3** In **Fig. 3a**, we can see that the raw reflectivity field is heavily contaminated with ground clutter and non-precipitation echoes, especially in the vicinity of the radar station. To eliminate out-of-the-ordinary signals from surface objects and atmospheric variability, a gate filter based on signal-to-noise ratio (SNR) thresholds (1-70 dB) was implemented using the free and open-source Py-ART package. With non-meteorological echoes properly suppressed, the precipitation structure is more clearly highlighted by the resultant filtered reflectivity (**Fig. 3c**). The next step was to implement attenuation correction in order to overcome the limitations of C-band radar. In places with heavy precipitation and at larger distances from the radar, the uncorrected reflectivity underestimates the rainfall intensity, as demonstrated in **Fig. 3d** Better detection of faraway and severe rainstorms is made possible by the restored signals brought about by the corrected field (**Fig. 3e**).

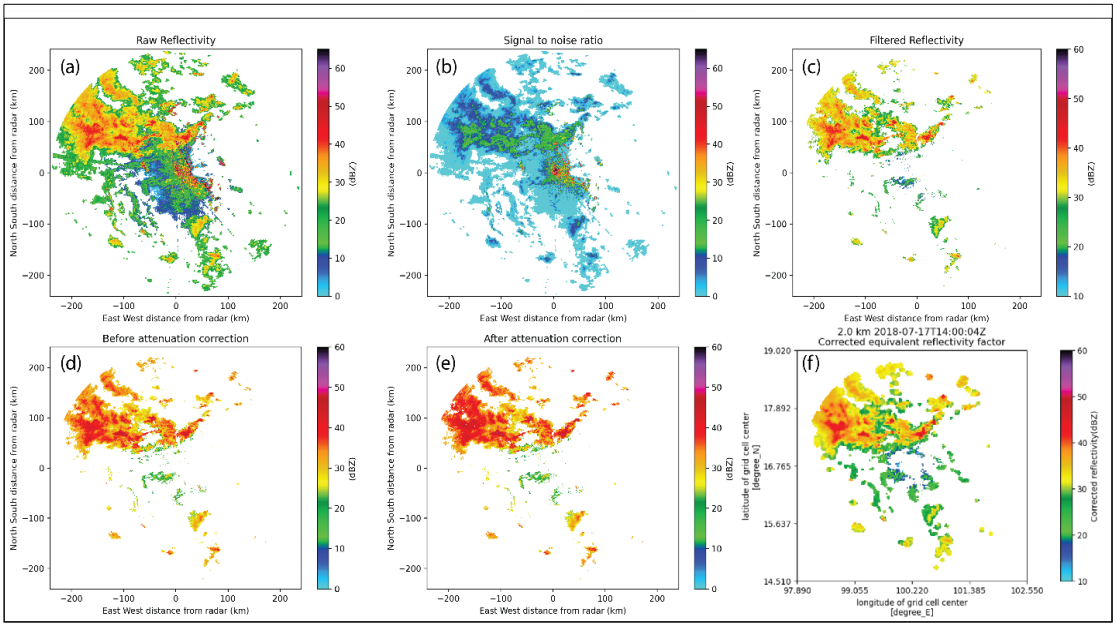

Fig. 3. Radar clutter and attenuation correction process during Tropical Storm Son-Tinh on 17 July 2018 at 21:00 local time (14:00 UTC). (a) Raw reflectivity, (b) Signal-to-Noise Ratio (SNR), (c) Filtered reflectivity using SNR-based gate filter, (d) Before attenuation correction, (e) After attenuation correction, (f) Conversion from polar coordinates to Cartesian grid. Reflectivity values are shown in the range of 0–60 dBZ.

Lastly, **Fig. 3f** shows the results of transforming the reflectivity data from polar to Cartesian coordinates. This created a gridded dataset that is spatially consistent and may be used for future rainfall estimation and analysis using GIS.

4.2. Development of the Radar Analysis Process in a GIS System

Using the open-source GIS program QGIS, which offers efficient capabilities for processing huge spatial datasets, the researchers in this work computed the accumulated rainfall on an hourly basis using radar measurements (Kangerd et al., 2024). Due to the complexity and lack of compatibility with spatial analysis in raw radar data, the reflectivity fields were converted into GIS-ready forms that could be used to integrate analytical models. For the purpose of reproducibility and adaptability in dealing with the massive amounts of data and high temporal resolution of radar scans, open-source software was chosen. The approach was optimized by using a QGIS automated processing model (**Fig. 4**).

Fig. 5 shows how this approach uses the three Z-R relationships to systematically transform raw reflectivity into hourly rainfall fields, which are then aggregated to create event-based rainfall datasets. The regional diversity induced by distinct Z-R relationships is illustrated in **Fig. 5**, which depicts the event-based accumulated rainfall during Tropical Storm Son-Tinh (15-23 July 2018). A no-data zone above the radar site was created by the cone of silence, and rainfall was scattered throughout most of the 120 km radar sweep.

The storm's most affected regions in the eastern and northeastern sectors also had the densest concentrations of heavy rainfall. The Z-R connections diverged significantly. The most intense rainfall was produced by the ZR-RF connection (**Fig. 5b**), which highlighted the presence of isolated convective cores. Strong rainfall was also recorded by the ZR-SD relationship (**Fig. 5c**), although it was less concentrated than ZR-RF. In comparison to the other two formulations, the ZR-MP relationship (**Fig. 5a**) produced a less concentrated and more evenly distributed rainfall field, which understated the severity of isolated extremes.

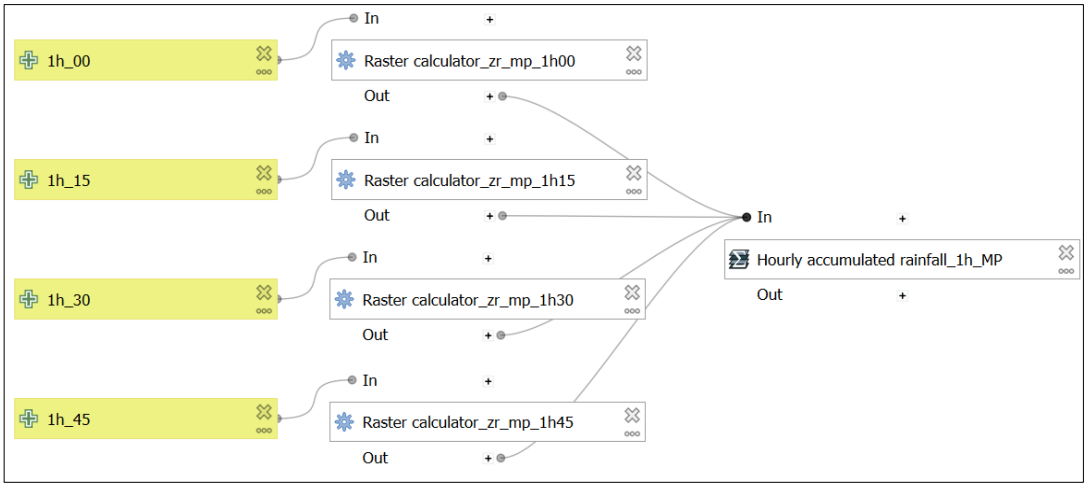

Fig. 4. Automated model for calculating hourly accumulated rainfall using the Marshall–Palmer Z–R relationship.

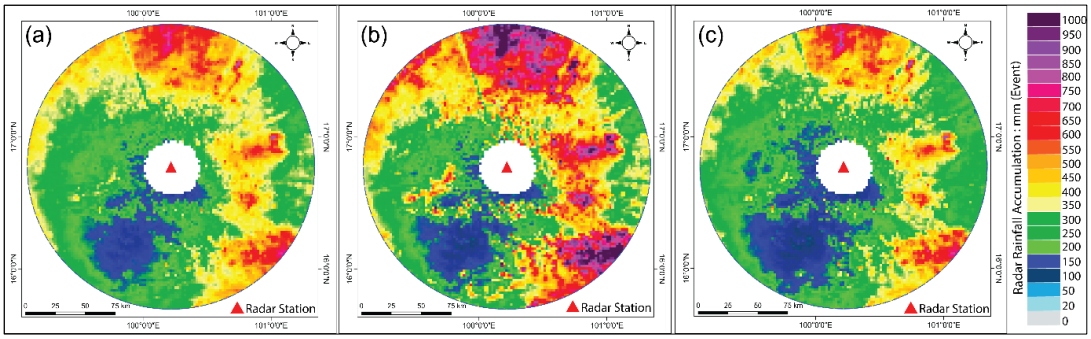

Fig. 5. Illustrates the event-based accumulated rainfall maps of Tropical Storm Son-Tinh from 15–23 July 2018 derived using different Z-R relationships: (a) ZR-MP, (b) ZR-RF, and (c) ZR-SD.

Rainfall measurements at test rain gauge locations (**Fig. 1b**) were obtained using radar-derived rainfall maps, retaining only nonzero pairs for analysis. This combination facilitated the computation of bias between radar and gauge data, subsequently spatially interpolated by the IDW method. **Fig. 6** provides an example of the interpolation findings for the ZR-MP connection. The bias distribution displays distinct spatial patterns: radar consistently overestimates rainfall in the eastern region of the coverage area (red shading) while underestimating rainfall in the mountainous west (blue shading), where topographic blockage diminishes radar signal reliability. While **Fig. 6** shows the ZR-MP scenario, same spatial bias tendencies were noted for the ZR-RF and ZR-SD correlations.

Following bias correction with the adjustment factors generated from the IDW, **Fig. 7** shows the rainfall fields locations where the radar had previously overestimated rainfall now have lower values, and locations where it had underestimated rainfall have had their value adjusted upwards to match gauge observations. This is clearly visible in the revised maps. By validating the results against separate stations, we can see that the correction process successfully reduced systematic deviations and confirmed a significant decrease in MBE. Because the bias's spatial distribution doesn't change over time, we can infer that the inaccuracies are systematic and caused mostly by differences in station placement and topography. One way to improve radar rainfall estimates is to use the spatially averaged bias as a correction factor. However, the distribution and density of rain gauges limit the precision of the corrections; in areas where there are few gauges, residual errors could be left over since the bias estimation isn't as accurate.

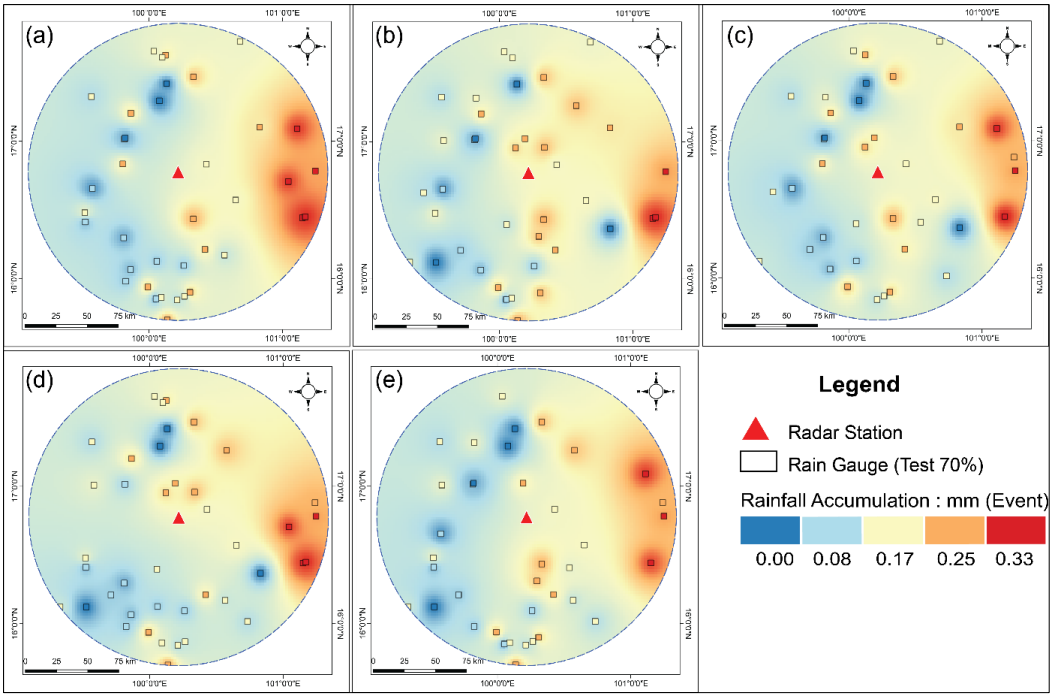

Fig. 6. Event-based spatial interpolation of bias using the IDW method derived from the Marshall–Palmer (ZR-MP) relationship, based on 70% of ground rain gauge stations used as the test set through K-fold cross-validation, with panels representing (a) K-fold = 1, (b) K-fold = 2, (c) K-fold = 3, (d) K-fold = 4, and (e) K-fold = 5.

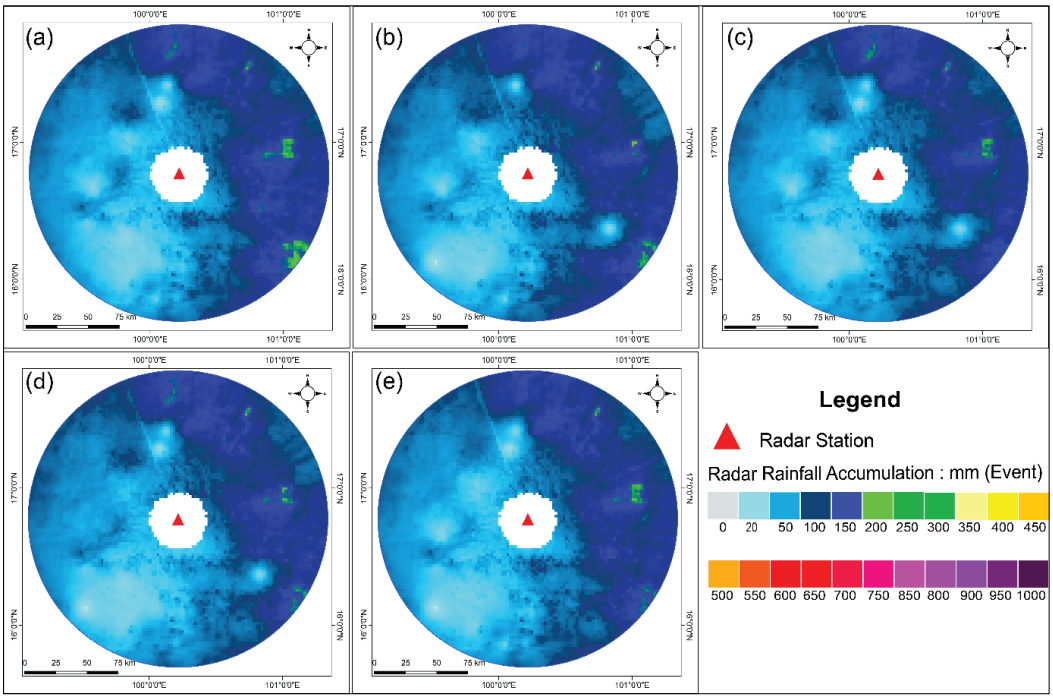

Fig. 7. Event-based radar rainfall maps after spatial bias correction using the IDW method, derived from the Marshall–Palmer (ZR-MP) relationship, with K-fold cross-validation applied, where (a) K-fold = 1, (b) K-fold = 2, (c) K-fold = 3, (d) K-fold = 4, and (e) K-fold = 5.

4.3. Spatial Bias Correction

Five-fold cross-validation (K = 5) was used to adjust MFB using rainfall values from test rain gauge locations. **Table 2.** shows that this procedure's estimations of Mean Rain Gauge, Mean Rain Radar, Bias, and MFB contain both geographical and temporal variability, and that it minimized dependent on a single train-test split by averaging findings across five rounds. Different behaviors were displayed by the three Z-R connections. The ZR-RF equation yielded the lowest Bias (0.115 mm), but it provided extremely high radar totals (331.333 mm compared to 37.047 mm from gauges), suggesting a significant overestimation that would skew estimations of cumulative rainfall. The ZR-SD relationship, on the other hand, reflected systematic underestimation by producing lower radar totals but the largest Bias (0.168 mm). The most balanced findings were produced by the ZR-MP relationship, which avoided significant overestimation while still providing accurate radar rainfall of 247.100 mm with a mild Bias of 0.150 mm. When it came to this event, ZR-MP consistently performed the best.

Table 2.

Adjustment of Mean Field Bias using k-fold cross validation.

k-fold cross validation	Mean Rain gauge (mm)	Mean Rain radar (mm)	Bias (mm)	MFB (mm)
Marshall/Palmer	37.047	247.100	0.150	37.047
Rosenfeld Tropical	37.047	321.334	0.115	37.047
Summer Deep Convection	37.047	220.003	0.168	37.047

The initial evaluation of the bias between radar-derived rainfall and gauge observations was conducted using the 30% validation set prior to correction. Substantial biases were observed in the northern and eastern sectors of the study area, particularly over mountainous terrain, as illustrated in **Fig. 8(a–e)** for the ZR-MP relationship. The largest deviations between radar and gauge values were observed in these regions, which were influenced by topographic factors such as anomalous propagation, beam obstruction, and signal attenuation. In contrast, the central lowlands exhibited relatively lesser biases, which is consistent with the more stable radar performance in flat terrain.

Discrepancies were substantially reduced throughout the study area following bias correction (**Fig. 8(f–j)**). The bias magnitudes in mountainous regions experienced a significant decrease, whereas the lowland areas exhibited only minor alterations as a result of their preexisting lower bias levels. The correction enhanced agreement with gauge data in all three Z–R relationships, although the degree of improvement differed. The residual biases of the ZR-RF and ZR-SD equations were higher than those of the ZR-MP equation, suggesting that the ZR-MP equation was more effective in reducing systematic errors. This result is in accordance with the results summarized in **Table 3.**, which indicate that ZR-MP exhibited the lowest average bias across K-folds and terrain categories.

The performance of the three Z–R equations—ZR-MP, ZR-RF, and ZR-SD—before and after bias correction is summarized in **Table 3.** The correlation and determination coefficients (R^2) for all three relationships were enhanced by the correction, which was implemented through IDW spatial interpolation with five-fold cross-validation. The most consistent results were obtained by ZR-MP, which also had the highest post-correction correlation (0.761) and R^2 (0.850) and an MBE of 0.999 mm, indicating excellent agreement with gauge observations.

ZR-SD, which initially exhibited the highest bias prior to correction, significantly improved following correction and nearly matched the performance of ZR-MP (Correlation = 0.757; R^2 = 0.848; MBE = 0.990 mm). Conversely, ZR-RF demonstrated inferior post-correction performance, as evidenced by its reduced correlation (0.729) and R^2 (0.829), despite its negligible pre-correction bias. In conclusion, these findings verify that bias correction employing IDW with cross-validation effectively mitigates systematic errors and enhances radar rainfall accuracy. The most balanced and reliable estimates were provided by ZR-MP, while ZR-SD exhibited significant post-correction potential. ZR-RF was less effective for this event.

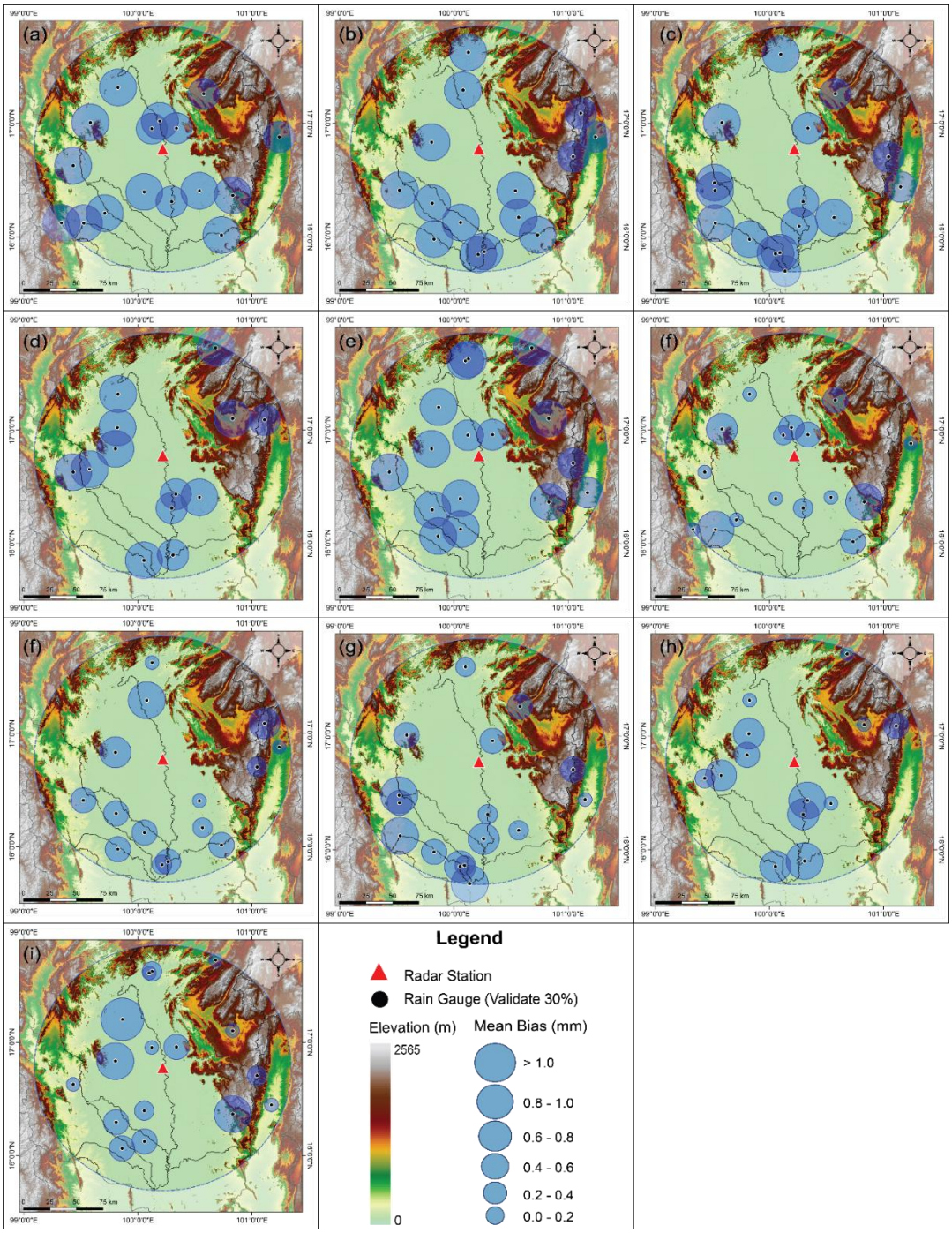

Fig. 8. Maps illustrating the bias between radar-derived rainfall and ground-based rain gauge measurements before (a–e) and after correction (f–j) using the bias values from the ZR-MP relationship, with K-folds as follows: K-fold=1 (a, f), K-fold=2 (b, g), K-fold=3 (c, h), K-fold=4 (d, i), and K-fold=5 (e, j).

Table 3.

Results Before and After Bias Correction of Validation Stations using k-fold cross validation.

Z-R Relationship	Correlation (mm)		R^2 (mm)		Mean Bias (mm)	
	Before	After	Before	After	Before	After
Marshall/Palmer	0.678	0.761	0.808	0.850	0.154	0.999
Rosenfeld Tropical	0.618	0.729	0.775	0.829	0.120	0.948
Summer Deep Convection	0.670	0.757	0.805	0.848	0.176	0.990

The error metrics (RMSE and MAE) for radar-derived rainfall that were compared to gauge observations before and after the application of IDW spatial bias correction are presented in **Table 4.** Confirming the efficacy of IDW interpolation in enhancing rainfall estimation accuracy, the correction significantly reduced errors across all Z–R relationships. ZR-MP demonstrated the most significant improvement among the three equations, with a reduction in RMSE from 218.186 mm to 17.517 mm and MAE from 199.004 mm to 13.405 mm. This represents the most significant error reduction overall. At first, ZR-RF exhibited the lowest pre-correction errors; however, its post-correction performance was marginally inferior to that of ZR-MP. This suggests that despite a robust baseline, ZR-RF has limited responsiveness to spatial bias adjustment. ZR-SD exhibited the highest pre-correction errors (RMSE = 309.163 mm; MAE = 265.412 mm). However, these values were reduced to 19.263 mm and 14.483 mm, respectively, by bias correction. Consequently, they remained higher than those of ZR-MP and ZR-RF. Overall, these results indicate that IDW spatial interpolation effectively mitigates systematic errors in radar rainfall estimates. Particularly, the ZR-MP equation demonstrated the most balanced enhancement, as it combined substantial error reductions with consistent agreement across terrain types.

Table 4.

Statistical Values Before and After Adjustment Using the IDW Spatial Interpolation Method.

Z-R Relationship	Before Correction		After correction	
	RMSE (mm)	MAE (mm)	RMSE (mm)	MAE (mm)
Marshall/Palmer	218.186	199.004	17.517	13.405
Rosenfeld Tropical	309.163	265.412	19.263	14.483
Summer Deep Convection	191.622	170.765	17.719	13.571

4.4. Analysis of Flat and Mountainous Rainfall Considering Topography

Utilizing a DEM-based classification, the bias correction performance was evaluated separately for flat and mountainous regions in order to evaluate terrain-related effects (**Fig. 9**). Slopes that were less than 5° were classified as level, while those that exceeded 5° were classified as mountainous. Then, statistical indicators of radar‑gauge agreement were computed for each terrain zone, allowing for the comparison of the efficacy of corrections in contrasting topographic conditions.

The mean radar-estimated rainfall for flat and mountainous areas is compared in **Fig. 10** before and **Fig. 11** after bias correction. The ZR-RF relationship produced the highest totals, followed by ZR-MP and ZR-SD, and all three Z–R relationships substantially overestimated rainfall prior to correction. The uncorrected radar estimates exhibit a significant degree of variability, as evidenced by the large error bars in both terrain types. The mean rainfall estimates decreased consistently across all relationships after the IDW bias correction was implemented, with reductions of approximately 60 mm in both flat and mountainous zones. Reduced variability and enhanced reliability of the corrected radar data were also indicated by the narrowing of the error bars. ZR-MP demonstrated the most statistically robust performance of the three equations, resulting in rainfall estimates that were most closely aligned with gauge observations and the lowest post-correction variability.

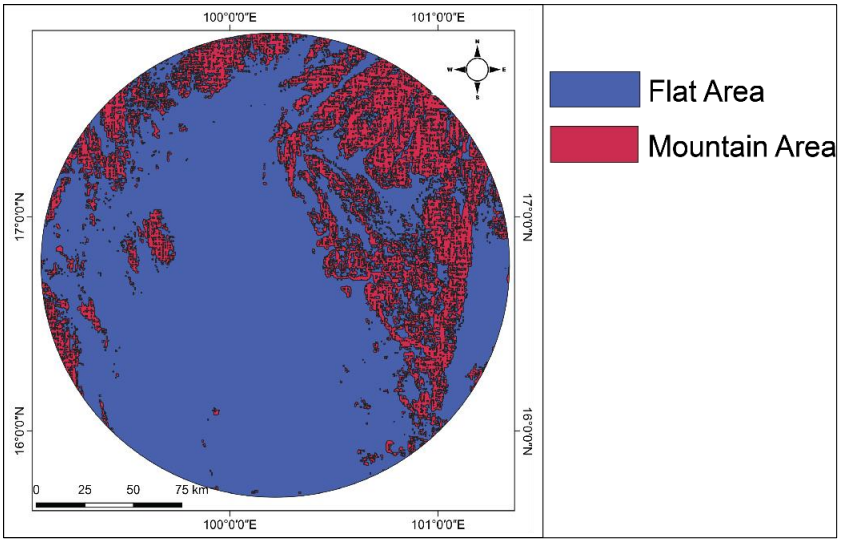

Fig. 9. Topographic map showing flat areas (slope ≤ 5°) and mountainous areas (slope > 5°).

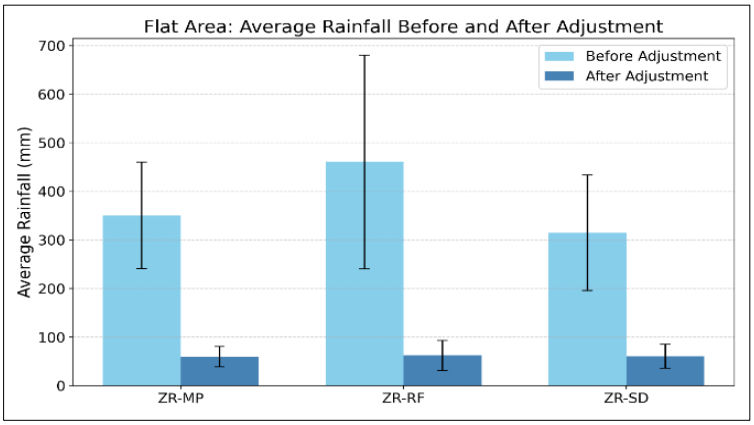

Fig. 10. Mean radar-estimated rainfall before spatial bias correction in flat areas and mountainous areas for the three Z-R relationships.

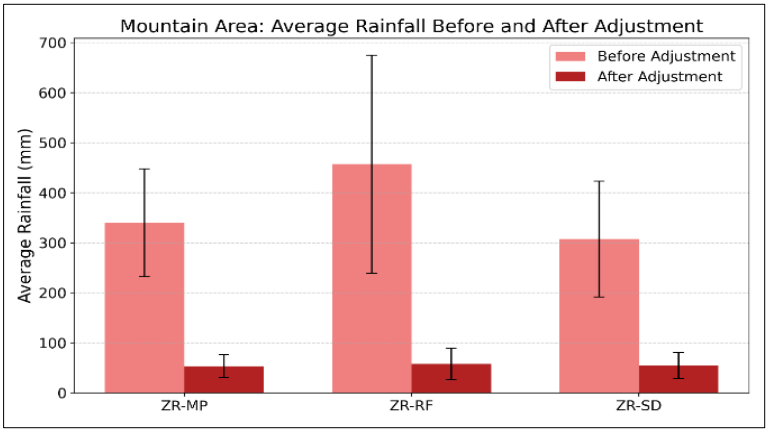

Fig. 11. Mean radar-estimated rainfall after spatial bias correction in flat areas and mountainous areas for the three Z-R relationships.

5. DISCUSSION

The suitability of various Z–R relationships for radar rainfall estimation and bias adjustment during Tropical Storm Son-Tinh (15–23 July 2018) over the central river basin of Thailand was assessed in this study. Radar data from the Phitsanulok C-band station were combined with gauge observations from 89 rain stations. Spatial bias correction was implemented using IDW, and accuracy was evaluated through five-fold cross-validation. The results emphasize the necessity of bias correction before the operational use of radar rainfall products, particularly in regions with complex terrain that encompasses both lowlands and mountainous areas. The analysis indicates that the selection of the Z–R relationship significantly impacts the accuracy of radar rainfall, which is in accordance with previous findings (Mahavik et al., 2021; 2025). ZR-MP relationship was the most dependable of the three equations that were tested, as evidenced by the firm agreement between post-correction performance and gauges ($r = 0.761$, $R^2 = 0.850$, and MBE ≈ 0.999 mm). The RMSE and MAE experienced considerable reductions in error, with the former decreasing to 17.517 mm and the latter to 13.405 mm. These results verify that the combination of ZR-MP and IDW bias correction produces highly dependable rainfall fields, which is in accordance with prior research (Goudenhoofdt & Delobbe, 2009; Mahavik, 2017; Mahavik et al., 2024; 2025).

In contrast, ZR-RF and ZR-SD initially appeared to perform better in terms of numerical bias; however, they both significantly overestimated rainfall. This may be indicative of the spatial and temporal variability of Z–R performance, which is indicative of variations in storm structure in relation to the conditions under which these relationships were established (Mapiam & Sriwongsitanon, 2008; Mahavik et al., 2011). The results also suggest that spatial bias correction has a more significant impact on the ultimate accuracy than Z–R selection. This study confirms that the accuracy of radar rainfall across diverse terrain is considerably enhanced by the application of spatial bias correction with IDW, which is supported by cross-validation. In addition to deterministic correction methods, the integration of machine learning with ground-based rainfall data presents a promising opportunity to further mitigate spatial bias and improve quantitative precipitation estimates (Hassan et al., 2022; Mihulet et al., 2023; Mahavik et al., 2024; 2025).

6. CONCLUSIONS

Using reflectivity data from the Phitsanulok C-band radar in Thailand and rain gauge observations, this investigation assessed the bias correction of event-based radar rainfall during Tropical Storm Son-Tinh (15–23 July 2018). Clutter and attenuation effects were effectively eliminated through data preprocessing with Py-ART, and rainfall was estimated using three Z–R relationships. Initially, all equations overestimated rainfall, with Rosenfeld Tropical leading to the largest deviations. Conversely, the Marshall–Palmer (ZR-MP) relationship provided the most balanced estimates. Spatial bias correction, as well as five-fold cross-validation and IDW, significantly enhanced radar–gauge agreement in both flat and mountainous regions. The most dependable performance was obtained by ZR-MP among the tested relationships, as evidenced by its significantly reduced errors and closer adherence to gauge measurements. These findings verify that it is imperative to incorporate a spatial bias correction and an appropriate Z–R relationship in order to enhance radar quantitative precipitation estimates in complex terrain. In order to improve radar rainfall estimation during tropical storm events in Thailand and similar monsoon-dominated regions, However, this study still has limitations regarding the number of rainfall observation stations, which may not be sufficient, and radar data that are affected by blockage due to terrain characteristics, remaining a constraint within the study area. For future research, the investigators suggest expanding the analysis to include more advanced techniques, such as comparing the IDW method with other bias correction and estimation approaches, including Kriging, co-Kriging, Bayesian adjustment, or machine learning-based methods. These approaches could potentially improve quantitative rainfall estimation in both mountainous and lowland areas, thereby supporting more effective flood prevention planning and rainfall management.

ACKNOWLEDGEMENTS

This work was supported by Naresuan University (NU) and the National Science, Research, and Innovation Fund (NSRF) under Grant No. N25A660467. Additional support was provided by the Fundamental Fund (FF), Naresuan University, under Grant No. R2569B057, and by the Appropriate Technologies for Waste Reuse and Management Research Unit.

REFERENCES

Abro, M. I., Zhu, D., Wei, M., Majidano, A. A., Khaskheli, M. A., Ul Abideen, Z., & Memon, M. S. (2019). Hydrological appraisal of rainfall estimates from radar, satellite, rain gauge and satellite–gauge combination on the Qinhuai River Basin, *China. Hydrological Sciences Journal*, 64(16), 1957–1971. https://doi.org/10.1080 /02626667 .2018.1557335

Ahrens, B. (2006). Distance in spatial interpolation of daily rain gauge data. *Hydrology and Earth System Sciences*, 10, 197–208. https://doi.org/10.5194/hess-10-197-2006

Battan, L. J. (1973). Radar observation of the atmosphere. University of Chicago: University of Chicago Press.

Bowden, J. H., et al. (2025). Stormy Subtropics and Stratiform South: Radar-Based Classification and Analysis of Australian Rainfall Events. *Journal of Geophysical Research*: Atmospheres. https://doi.org/10.1029/2024JD041790

Brauer, C.C., Overeem, A., Leijnse, H., and Uijlenhoet, R. (2016). The effect of differences between rainfall measurement techniques on groundwater and discharge simulations in a lowland catchment. *Hydrological Process*, 30(21), 3885-39000.

Chang and Kang-tsung. (2002). Introduction to Geographic Information Systems. New York: *McGraw Hill Higher Education*.

Chen, F. W., & Liu, C. W. (2012). Estimation of the spatial rainfall distribution using inverse distance weighting (IDW) in the middle of Taiwan. *Paddy and Water Environment*, 10(3), 209–222.

Cho, Y. (2020). Application of NEXRAD radar-based quantitative precipitation estimations for hydrologic simulation using ArcPy and HEC software. *Water*, 12(1), 273. https://doi.org/10.3390/w12010273

Goudenhoofdt, E., & Delobbe, L. (2009). Evaluation of radar-gauge merging methods for quantitative precipitation estimates. Hydrology and Earth System Sciences, 13(2), 195–203. https://doi.org/10.5194/hess-13-195-2009

Gourley, J. J., & Calvert, C. M. (2003). Automated Detection of the Bright Band Using WSR-88D Data. *Weather and Forecasting*, 18(4), 585-599. https://doi.org/10.1175/1520-0434(2003)018<0585:ADOTBB>2.0.CO;2

Gu, J., Ryzhkov, A., Zhang, P., Neilley, P., Knight, M., Wolf, B., & Lee, D. (2011). Polarimetric Attenuation Correction in Heavy Rain at C Band. *Journal of Applied Meteorology and Climatology*, 50(1), 39-58. https://doi.org/10.1175/2010JAMC2258.1

Hanchoowong, R., Weesakul, U., and Chumchean, S. (2012). Bias correction of radar rainfall estimates based on a geostatistical technique. *Science Asia*, 38(4), 373–385.

Harrison, D., Smith, J., and Brown, P. (2009). Exploring the Transient Behavior of Z–R Relationships: Implications for Radar Rainfall Estimation. *Journal of Applied Meteorology and Climatology*, 48(10), 2055–2067. https://doi.org/10.1175 /2009JAMC2165.1

Hassan, D., Isaac, G. A., Taylor, P. A., & Michelson, D. (2022). Optimizing Radar-Based Rainfall Estimation Using Machine Learning Models. *Remote Sensing*, 14(20), 5188. https://doi.org/10.3390/rs14205188

Helmus, J. J., and Collis, S. M. (2016). The Python ARM Radar Toolkit (Py-ART), a library for working with weather radar data in the Python programming language. *Journal of Open Research Software*, 4(1), Article e25. https://doi.org/10.5334/jors.119

Kangerd, A., Mahavik, N., Masthawee, F., Arthayakun, S., Ket-Ord, R., Samaksaman, U., Umponstira, C., Kunwilai, J., Promta, W., Kongmuang, C., and Tantanee, S. (2024, November 17–21). Analysis of spatial bias of precipitation estimated from weather radar data during storm dissipation with geographic information system in Central Thailand. *Paper presented at the 45th Asian Conference on Remote Sensing (ACRS 2024)*, Colombo, Sri Lanka.

Krajewski, W. F., & Smith, J. A. (2002). Radar hydrology: Rainfall estimation. *Advances in Water Resources*, 25(8–12), 1387–1394. https://doi.org/10.1016/S0309-1708(02)00062-3

Krajewski, W. F., Vignal, B., Seo, B.-C., & Villarini, G. (2011). Statistical model of the range-dependent error in radar–rainfall estimates due to the vertical profile of reflectivity. *Journal of Hydrology*, 402(3–4), 306–316. https://doi.org/10.1016/j.jhydrol.2011.03.024

Krajewski, W. F., Villarini, G., & Smith, J. A. (2010). Radar–rainfall uncertainties: Where are we after thirty years of effort?. *Bulletin of the American Meteorological Society*, 91(1), 87–94.

Lin XS, Yu Q (2008) Study on the spatial interpolation of agroclimatic resources in Chongqing. *J Anhui Agric* 36(30): 13431–13463, 13470

Mahavik, N. (2017). Bias adjustments of radar rainfall during seasonal march of the summer monsoon in the middle of Thailand. *International Journal of Applied Environmental Sciences*, 12(4), 577-594.

Mahavik, N., & Tantanee, S. (2020a). Radar Quality Index for a mosaic of radar reflectivity over Chao Phraya River Basin, Thailand. *Applied Environmental Research*, 42(3), 92‑104.

Mahavik, N., Kangerd, A., Masthawee, F., Arthayakun, S., and Tantanee, S. (2025). Optimizing rainfall prediction in central Thailand with weather radar and machine learning during the monsoon. *Environmental Earth Sciences*, 84(137). https://doi.org/10. 1007/s12665-025-12149-9

Mahavik, N., Kangerd, A., Masthawee, F., Arthayakun, S., and Tantanee, S. (2024). Investigate ensemble machine learning models to reduce the daily mean field bias of radar rainfall estimates derived from ZR relationships in the sub-river basins in the middle of Thailand. *Environment, Development and Sustainability*. https://doi.org/10.1007/s10668-024-05778-w

Mahavik, N., Masthawee, F., Tantanee, S., (2021). Investigation Z-R relationships during tropical storm in GIS using implemented mosaicking algorithms of radar rainfall estimates from weather radars in the Yom river basin, *Thailand. Applied Geomatics*. 13, 645-657.

Mahavik, N., Satomura, T., and Baimuang, S. (2011). Investigation Z–R relationships of precipitation characteristic by weather radar in Thailand. *In Proceedings of the IMPAC-T Joint with SEA Water 9th Conference* (pp. 212–217). Bangkok, Thailand.

Mahavik, N., Tantanee, S., (2020b). Precipitating clouds analysis based on the developed radar mosaic products over the Chao Phraya River basin. *International Journal of Geoinformatics*, 16(3), 21-35.

Mapiam, P. P., and Sriwongsitanon, N. (2008). Climatological Z-R relationship for radar rainfall estimation. *ScienceAsia*, 34, 215-222. https://doi:10.2306/scienceasia1513-1874.2008.34.215

Mapiam, P. P., Methaprayun, M., Bogaard, T., Schoups, G., & Ten Veldhuis, M.-C. (2022). Citizen rain gauges improve hourly radar rainfall bias correction using a two-step Kalman filter. *Hydrology and Earth System Sciences*, 26(3), 775–794.

Marshall, J.S. and Palmer, W.M. (1948). The distribution of raindrops with size. *Journal of Atmospheric Sciences*, 5(6), 165–166

Marshall, J.S., Walter, H., and Gunn, K.L. (1955). Advances in radar weather. *Advances in Geophysics*, 2, 1-56.

Mihulet, E., Burcea, S., Mihai, A., & Czibula, G. (2023). Enhancing the Performance of Quantitative Precipitation Estimation Using Ensemble of Machine Learning Models Applied on *Weather Radar Data. Atmosphere*, 14(1), 182. https://doi.org/10.3390/atmos14010182

Mokarram, M., & Hojati, M. (2016). Comparison of landform classifications of elevation, slope, relief and curvature with topographic position index in south of Bojnoord. *Ecopersia, 4*(2), 1343–1357. https://doi.org/10.18869/modares.Ecopersia.4.2.1343

Morin, E., Krajewski, W. F., Goodrich, D. C., Gao, X., & Sorooshian, S. (2003). Estimating rainfall intensities from weather radar data: The scale-dependency problem. *Journal of Hydrometeorology*, 4(5), 782–797. https://doi.org/10.1175/1525-7541(2003)004<0782:ERIFWR>2.0.CO;2

National Water Resources Office. (2018). 20-year master plan for water resource management (2018-2037).

QGIS Development Team. (2024). QGIS Geographic Information System (Version 3.34). QGIS Association. https://qgis.org

Rosenfeld, D., Wolff, D. B., and Atlas, D. (1993). General probability-matched relations between radar reflectivity and rain Rate. *Journal of Applied Meteorology Climatology*, 32(1), 50–72.

Sharif, R. B., Habib, E. H., & ElSaadani, M. (2020). Evaluation of radar-rainfall products over coastal Louisiana. *Remote Sensing*, 12(9), 1477. https://doi.org/10.3390/rs12091477

Sokol, Z., Szturc, J., Orellana-Alvear, J., Popová, J., Jurczyk, A., & Célleri, R. (2021). The role of weather radar in rainfall estimation and its application in meteorological and hydrological modelling A review. *Atmosphere*, 13(3), 351.

Thai Meteorological Department. (2018). Member report: Thailand. ESCAP/WMO Typhoon Committee, 13th Integrated Workshop, Chiang Mai, Thailand. https://www.jma.go.jp/jma/en/Activities/qmws_2010/docs/Workshop_ver0.98_ins.pdf

World Meteorological Organization. (2008). Guide to hydrological practices: Volume I. Hydrology ‐ From measurement to hydrological information (6th ed.) (WMO-No. 168). World Meteorological Organization. https://unstats.un.org/unsd/envaccounting/waterGuidelines/Material/WMO_Guide_168_Vol_I_en_hydrological_practices.pdf

Wu, W., Zou, H., Shan, J., & Wu, S. (2018). A dynamical Z–R relationship for precipitation estimation based on radar echo-top height classification. *Advances in Meteorology*, 2018, Article 8202031. https://doi.org/10.1155/2018/8202031

Xie, H., Zhou, X., Vivoni, E. R., Hendrickx, J. M. H., & Small, E. E. (2005). GIS-based NEXRAD Stage III precipitation database: Automated approaches for data processing and visualization. *Computers & Geosciences*, 31(1), 65–76.